Journal of Nuclear Materials 542 (2020) 152458

Contents lists available at ScienceDirect

Journal of Nuclear Materials

journal homepage: www.elsevier.com/locate/jnucmat

Effects of minor alloying addition on He bubble formation in the irradiated FeCoNiCr-based high-entropy alloys

Da Chen[a,b], Shijun Zhao[a,b,*], Jianrong Sun[c,d,**], Pengfei Tai[c,d], Yanbin Sheng[c,d], Guma Yeli[a,b], Yilu Zhao[a,b], Shaofei Liu[a,b], Weitong Lin[a,b], Wu Kai[e], Ji-Jung Kai[a,b,*]

[a] Department of Mechanical Engineering, City University of Hong Kong, Hong Kong, China
[b] Centre for Advanced Nuclear Safety and Sustainable Development, City University of Hong Kong, Hong Kong, China
[c] Institute of Modern Physics, Chinese Academy of Sciences, Lanzhou 710000, China
[d] School of Nuclear Science and Technology, University of Chinese Academy of Sciences, Beijing 100049, China
[e] Institute of Materials Engineering, National Taiwan Ocean University, Keelung 20224, Taiwan, ROC

ARTICLE INFO

Article history:
Received 26 April 2020
Revised 23 July 2020
Accepted 10 August 2020
Available online 14 August 2020

Keywords:
High-entropy alloy
Minor alloying
Helium bubble
Vacancy migration
Phase stability

ABSTRACT

Minor alloying with specific elements is an effective approach to tailor material's properties, but it has not been introduced to modify the radiation effects of high-entropy alloys (HEAs), which are a promising material for nuclear application. In the work, a 0.2 molar ratio of Al/Cu/Ti was respectively added into the quaternary FeCoNiCr HEA, they were then irradiated by 2 MeV He ions at four temperatures from 673 to 973 K. After irradiation, He bubble behavior in specimens were investigated by the transmission electron microscopy (TEM). The results showed that bubbles in the minor alloying HEAs usually had a larger size, lower number density, and broader distribution range, comparing to their parent alloy. Such effects were more significant at a higher irradiation temperature and most pronounced by the Ti-addition. Atomistic simulations revealed that such minor alloying addition could relatively reduce the energy barrier for vacancy migration and formation in FeCoNiCr system, which thereby promotes He diffusion through the replacement or vacancy mechanism. The theoretical models for He bubble formations verified our results that a higher He diffusivity in the minor alloying HEAs can enhance bubble growth and lower its nucleation numbers during irradiation. The phase stability of irradiated HEAs were also examined and its potential influences on bubble evolution were pointed out. This study provides insights on tailoring radiation defects via the conventional alloying strategy.

Introduction

Developing the novel structural materials which can withstand the extreme radiation environment has been a great challenge for the implementation of next generation nuclear systems [1]. In the beginning of this century, a new class of high-entropy alloy (HEA) composing with four or more principal elements in equal-molar or near equal-molar constituents [2,3], opened a new world for alloy design. Recent studies showed that the concentrated solid-solution HEAs had a better radiation resistance comparing to the simple metallic systems [4–6], which has drawn great interests in the nuclear material community. Fundamentally different from the dilute alloys, the local environment surrounding each atom is unique in HEAs [7]. As a result, the local-structure-dependent properties, such as defect formation and migration energies, exhibit fluctuations [8–10]. It has been proposed that such fluctuations might benefit the radiation resistance of HEAs [11], in which the rough energy landscapes can alter the mobility of defects, and finally enhance the recombination of *Frenkel* pairs.

Minor alloying with specific elements is a traditional method to optimize the properties of metallic material. For the radiation purpose, it has been reported that the small addition of Ti, Al, Si, Hf, Zr, etc. can modify the evolution of radiation defects in austenite alloys [12–15], e.g. adding the oversized element (Hf, Zr, Ta, Nb, Ti, V) into solution annealed 316L austenitic steels can retards void swelling through extending the incubation period for void nucleation and suppressing the void growth [12]. Mazey and Hanks also reported that the solute additions of 0.25%Si or 1.2% Ti into the model alloy with base compositions as the matrix phase of PE16, could reduce the void swelling, whereas the 1.2% Al-addition

* Corresponding authors at: Department of Mechanical Engineering, City University of Hong Kong, Hong Kong, China.
** Corresponding author at: Institute of Modern Physics, Chinese Academy of Sciences, Lanzhou 710000, China.
E-mail addresses: shijzhao@cityu.edu.hk (S. Zhao), sunjr@impcas.ac.cn (J. Sun), jijkai@cityu.edu.hk (J.-J. Kai).

https://doi.org/10.1016/j.jnucmat.2020.152458
0022-3115/

Table 1
Ion irradiation conditions for the FeCoNiCr-based HEAs.

Ions	2 MeV He^+ to a fluence of 1.52 × 10^{20} ions/m^2			
Temperature (K)	673	773	873	973
Peak damage / He concentration	~0.3 dpa / 6831 appm			
Time consumed (s)	3480–3600			
Materials	FeCoNiCr and FeCoNiCr(Al/Cu/Ti)$_{0.2}$ HEAs			

would markedly increase it [15]. Some speculations on this phenomenon were linked to the changed mobility of point defects in the matrix [16]. Therefore, it is instructive to further tailor the radiation effects of HEAs using this strategy. Among the hundreds of multicomponent systems [17], FeCoNiCr-based HEAs belonging to the family of 3-*d* transition metals have been demonstrated an excellent mechanical property over a wide temperature range [18–20], great corrosion/oxidation resistance [21,22], and promising radiation damage tolerance [23–25]. Chen et al. [26] found that the Ti-addition in FeCoNiCr HEA can delay the transformation of faulted dislocation loop via lowering the stacking fault energy of system, while the $L1_2$ phase could simultaneously precipitate at 400 °C irradiation. Zhang et al. [27] investigated the thermal and irradiation stability of nanocrystalline CoCrCuFeNi HEA, they found that the secondary phase appeared at 500 °C annealing. Yang et al. [28] irradiated the solid solution $Al_{0.3}$CoCrFeNi at temperatures from 250 °C to 650 °C, in which various dislocation structures developed and radiation enhanced diffusion could assist the precipitation of $L1_2$ phase and B_2 phase. These studies advanced our knowledges on the radiation effects of FeCoNiCr-based HEAs but failed to give a comprehensive understanding on the roles of minor alloying elements.

For the high Ni-content alloy applied in the fast neutron reactors, extensive helium (He) transmutation reactions can induce the considerable bubble structures which will lead to a He embrittlement at the high-temperature service [29–31]. As a vacancy-type radiation defect, He bubble formation is highly controlled by the mobility and abundance of vacancies in materials. Hence, it can be a desirable "prober" to measure the possible variation of energy landscape in materials. Our previous studies have found that the simple quaternary FeCoNiCr HEA has a stronger bubble formation resistance comparing to the pure Ni [32–34], in which He diffusion and accumulation was suppressed by the featured energetics of point defects in the multicomponent system. Based on these considerations, we designed this study combing He^+ irradiation experiments and atomistic simulations, to explore the minor alloying effects of Al, Cu, and Ti on He bubble formation in the FeCoNiCr-based HEAs. The bubble behaviors including its distribution range, size and number density were carefully investigated by the transmission electron microscopy (TEM). The energy landscapes of vacancies in the above systems were evaluated by molecular dynamics (MD) simulations using the proper potentials. Phase stability of irradiated HEAs were also examined and its potential influence on He bubble evolution were suggested.

Methodology

Materials and irradiation

Previous metallurgical studies on the FeCoNiCr system have suggested that further alloying by Al, Cu or Ti can affect the phase stability of parent alloy [35–37]. To stabilize the investigated materials, 0.2 molar ratio seems to be an upper bound of minor alloying concentration for the FeCoNiCr HEA. In this work, the HEAs with a composition of FeCoNiCr(Al/Cu/Ti)$_{0.2}$ were selected as the target materials, they were produced by the conventional arc-melting method in an argon atmosphere. Before irradiation, the as-cast alloys were all given a solid solution (SS) treatment at 1373 K for 5 h followed by water quenching. Then only the FeCoNiCr(Ti)$_{0.2}$ HEA was aged at 1073 K for 24 h, to further stabilize its phase structures during elevated-temperature irradiation. The irradiated specimens were first ground through 1200-grit SiC paper, then polished in a chemical suspension of 20 nm colloidal silica. The irradiation surface was finally mirror-like. The 2 MeV He^+ irradiation experiments were conducted at the material terminal of Low Energy Heavy Ion Accelerator Facility (LEAF) in Institute of Modern Physics, Chinese Academy of Sciences (IMP, CAS). The specimens were irradiated to a fluence of 1.52 × 10^{20} ions/m^2 at 673, 773, 873 and 973 K, respectively. During irradiation, He^+ beam flux was controlled at ~4.37 × 10^{16} ions/m^2s, while temperature was controlled within the error of ±5 K and vacuum of the irradiation chamber was maintained below 5.0 × 10^{-5} Pa. In order to get a homogeneous irradiation region, a raster beam was scanning with frequency of 200 Hz for the horizontal and vertical direction. The stopping and range of ions in matter program (SRIM-2010) [38] was adopted to predict the irradiation damage and He concentration along incident direction. In this simulation, the quick Kinchin-Pease mode was chosen according to suggestions from Stoller et al. [39] and the displacement energy was set as 40 eV for all target elements. The ion irradiation conditions were summarized in Table 1.

Post-irradiation characterization

Post irradiation, the cross-sectional TEM samples were prepared by the focused ion beam (FIB) of FEI Scios Dual Beam system, using the standard lift-out method [40]. To mitigate the artificial damage during milling process, the TEM lamellae were finally cleaned by low energy Ga^+ at 2 keV for 120 s. TEM characterizations were conducted using a JEM-2100F (JEOL) operated at 200 keV. Based on the Fresnel contrast mechanism, He bubbles were detected using the through-focus method. The phase stability of irradiated samples was examined by the selected area electron diffraction (SAED). To quantify the number density of bubbles observed in the 2-D projection of TEM image, the thickness of TEM film at the region of interest was measured by the two-beam convergent beam electron diffraction (CBED) patterns [41], which varied from 80–120 nm in this work. To guarantee the statistical significance, the number density was manually counted from 5 different locations with an area of 100 × 100 nm, the average bubble size was obtained from at least 100 bubbles. In addition, the nanofeatures of Cu-rich phase in Cu-addition HEA irradiated at 973 K was analyzed by the Atom probe tomography (APT), using a Cameca LEAP 5000XR instrument. Voltage pulsing with 20% pulse fraction was chosen. The specimen temperature and pulse repetition rate were set to 60 K and 200 kHz, respectively. CAMECA IVAS software was used to reconstruct the atomic information into 3D positions.

Atomistic simulation

Because of the extreme chemical complexity in the multicomponent system, full *ab initio* calculations are not feasible to obtain an overview of the alloying effects, in which lots of configurations need to be sampled. Therefore, calculations are carried out based

on the empirical potentials in this work. All simulations were performed using the open-source Large-scale Atomic/Molecular Massively Parallel Simulator (LAMMPS) code [42]. The interatomic interactions were described by the Embedded-Atom Method (EAM) parameterized by Zhou et al. [43] for Ni, Co, Fe, Al, Cu, and Ti elements and Lin et al. [44] for Cr. The mixing scheme proposed in [43] was used to model the interaction between different elements. As pointed out previously, the original version of the Cr potential leads to instabilities in alloys. Therefore, slight modification was made to the parameterization of Cr potential based on the analysis of Anand et al. [45]. This parametrization has been used to model defect accumulation and defect cluster (dislocation) properties in a series of concentrated alloys previously [46–49]. It also allows for a unified description of these different metallic elements.

Defect energetics including vacancy formation and migration energies, were calculated within an $8 \times 8 \times 8$ *fcc* supercell. The simulation box was populated randomly with Ni, Co, Fe and Cr atoms with equiatomic compositions initially. The defect formation energy was calculated by $E_f = E - E_0 \pm \mu_i$, where E is the energy of defective supercell, E_0 is the energy of pristine supercell, and μ_i is the chemical potential of the deleted or added elements (i). Here μ_i is calculated as the energy per atom in their bulk pure metals. The migration energies of defects were calculated by the climbing-image nudged-elastic-band (CI-NEB) method [50] as implemented in LAMMPS. A 'quick-min' damped minimization algorithm with a time step of 0.01 fs were adopted, and the convergence criteria of force was set to be 10^{-6} eV/Å. During the simulations, 12 intermediate images were used. The diffusion coefficients of a single vacancy were calculated using molecular dynamics (MD) simulations at different temperatures. The simulation was performed in a $10 \times 10 \times 10$ *fcc* supercell with periodic boundary conditions along all three directions, with an atomic composition of $(FeCoNiCr)_{0.95}$:$X_{0.05}$ (X: doping element).

Results

In this study, there are four kinds of specimens irradiated at four temperatures. Before the experimental results were comparatively presented, a demonstration for how we investigate the radiation effects was provided as follow. According to the results of SRIM simulation, the displacement damage and He concentration in 2 MeV He^+ irradiated FeCoNiCr HEA were calculated as a function of irradiation depth, showing in Fig. 1. For the $FeCoNiCr(Al/Cu/Ti)_{0.2}$ HEAs, the minor alloying addition would not give evident changes to the SRIM prediction, in which the created vacancies and injected He ions were nearly identical for the four alloy systems. Thus, the obtained profiles of radiation damage and He concentration could be taken as the same for them. To examine the depth dependence of radiation damage on microstructures, a low-magnification TEM image for the $FeCoNiCrAl_{0.2}$ HEA irradiated at 773 K was cropped from sample surface to a depth of ~4 um and attaching below the SRIM profiles in Fig. 1. The image shows some dark contrasts in the range of 3.0–3.5 um, roughly corresponding to the peak damage region predicted by SRIM. In general, there are two types of radiation defects observed in the damage region, as He bubbles and dislocation loops. The dark contrasts are believed to be caused by the strain fields surrounding these defects. Since the work mainly concerned the He bubble evolution along temperature effects and aimed to explore the effects of minor alloying on bubble behavior. In the lower images of Fig. 1, He bubbles showing the Fresnel contrasts were characterized by the through-focus TEM imaging. It can be found that the nanoscale He bubbles densely formed in the peak damage region of $FeCoNiCrAl_{0.2}$ HEA at 773 K. During elevated-temperature irradiation, the displacement damage and radiation enhanced diffusion would exert a synergetic effect on the phase stability [51]. The possible precipitation or dissolution might affect He bubble formation in the FeCoNiCr-based alloys. The inset SAED pattern in the middle image of Fig. 1 is to identify the phase constitutes in the peak damage region. It was acquired along zone axis of <011> and indicating a pure *fcc* structure for the $FeCoNiCrAl_{0.2}$ HEA irradiated at 773 K. In addition, it should be declared that all the following investigations were performed within grain of the well-annealed specimens, in which grain size (100–400 um) was large enough comparing to the penetration depth of He ions and the initial dislocation density was very low ($< 10^8$ /cm^2).

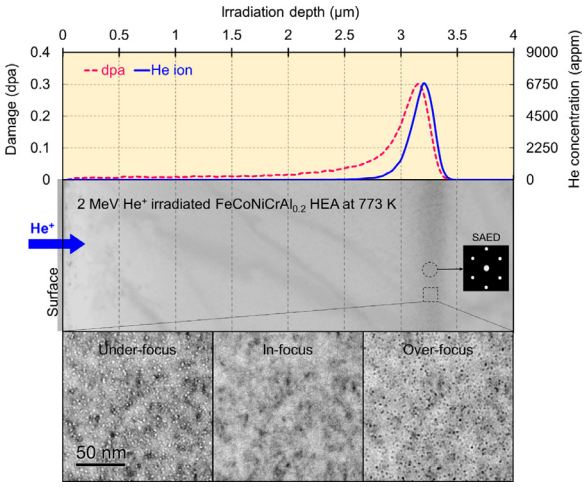

Fig. 1. A demonstration for characterization of $FeCoNiCrAl_{0.2}$ HEA irradiated by 2 MeV He^+ at 773 K. The upper graph shows the profiles of radiation damage and He concentration, which were calculated from the SRIM simulation results and plotted as a function of depth. The middle graph is a TEM image showing the overview of microstructures from sample surface to a depth of ~4 um, the inset SAED pattern was acquired from the peak damage region. The lower TEM images show the He bubbles in the denoted region, which imaging using the through-focus method.

Phase stability after irradiation

Prior to irradiation, a solid solution treatment on FeCoNiCr parent alloy and $FeCoNiCr(Al/Cu)_{0.2}$ HEAs was aimed to make a homogeneous *fcc* matrix for He bubble nucleation. Since our previous study has found that the minor Ti-addition could thermally precipitate the $L1_2$ phase in FeCoNiCr system even at a relatively low temperature irradiation [26], we conducted a pre-ageing treatment to give it the maximum thermal stability during irradiation. The microstructure of γ' precipitated strengthened $FeCoNiCr(Ti)_{0.2}$ HEA had been carefully reported in [52]. After irradiation at different temperatures, the phase stabilities of HEAs were examined at the peak damage region, where He bubble investigation was performed in the following section. In Fig. 2, a series of SAED patterns for different samples were all taken along the zone axis of <011> with the same camera length. The results indicate that the FeCoNiCr and $FeCoNiCr(Al/Cu)_{0.2}$ HEAs still kept their pure *fcc* structure, and no other phases contributed the reflection in the SAED patterns. For the $FeCoNiCrTi_{0.2}$ HEA, the superlattice diffraction spots of $L1_2$ phase were clearly observed, but their brightness slightly dimmed with decreasing temperature. It means the ordering structure of $L1_2$ phase was more susceptible to the radiation damage at a lower temperature. Our recent work has systematically addressed this issue and suggested that the same γ' precipitate could be sustained up to ~5 dpa at 673-873 K [53].

In general, the addition of Al into FeCoNiCr system has a chance to induce the formation of intermetallic compounds at a proper ageing condition [17], but the precipitation was controlled by the factors of the addition amount, aging temperature and time. He et al.

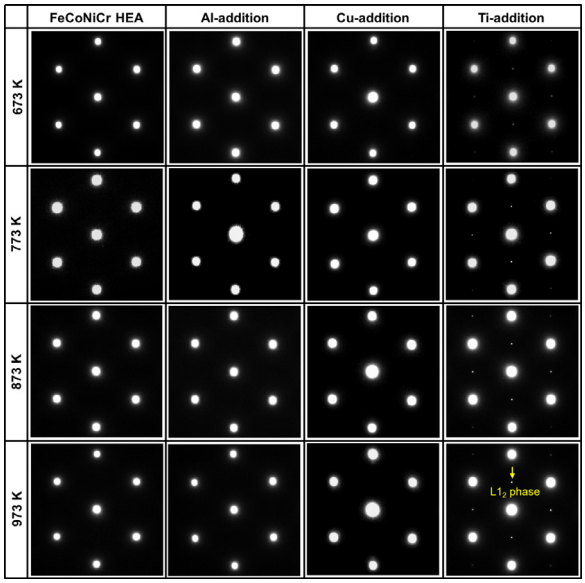

Fig. 2. The selected area electron diffraction (SAED) patterns for the peak damage region of FeCoNiCr-based HEAs irradiated at different temperatures. All the SAED were taken along the zone axis of <011>.

reported that the addition of Al with 0.1 molar ratio might induce a very small quantity of σ-phase when aging at 750 °C for 800 h [54]. As the addition was increased to 0.3 molar ratio, the Al can cause the formation of fine $L1_2$ phase at 550 °C for 150 h and B_2 phase at 700 °C for 50 h [35]. Yang et al. [28] also reported that the radiation enhanced diffusion could accelerate the precipitation of $L1_2$ phase and B_2 phase in the solid solution $FeCoNiCrAl_{0.3}$ HEA irradiated at 250–650 °C. In our case, the short exposing time (~1 h) and low radiation dose (~0.3 dpa) might be the two reasons for the stable $FeCoNiCrAl_{0.2}$ HEA, in which the dynamics required for phase transformation was not enhanced so much and the time was also inadequate for the kinetics.

For the Cu-addition, the quinary FeCoNiCrCu HEA exhibited a phase separation [55], that two kinds of *fcc* structures (FeCoNiCr-rich and Cu-rich) could form in the as-cast state. The similar behavior was also reported in the aged $FeCoNiCrCu_{0.5}$ HEA [36]. Since the Fe and Cu are mutually exclusive in thermodynamics, Cu-segregation might happen in our system while such nanofeatures are hardly captured by the conventional TEM method. In Fig. 3, an APT analysis was performed for the $FeCoNiCrCu_{0.2}$ HEA irradiated at 973 K. The sample was acquired in the peak damage region, where we can see the Cu-rich nanoclusters densely distributed. The clusters have an average size less than 4 nm in diameter (determined by the 10 at% Cu iso-concentration surface) and their number density reaches up to the magnitude of ~$10^{24}/m^3$. In addition to these nanoclusters, large-scale phase separation did not show in our sample. The reason should be attributed to the less Cu-addition (~4.7 at% in our case) comparing to the referred systems. The APT investigation on the Cu-lean phase of FeCoNiCrCu HEA [55] suggested that Cu had a solubility of ~10 at% in the FeCoNiCr system. Considering the indication of SAED pattern, the Cu-rich nanoclusters are believed as the nature of solute clusters, rather than a new phase with the distinct lattice structure. Overall, the irradiated HEAs all kept their pristine phase structures after irradiation, that the solution annealed FeCoNiCr and $FeCoNiCr(Al/Cu)_{0.2}$ HEAs still exhibited the simple FCC structure and the pre-aged $FeCoNiCrTi_{0.2}$ HEA also showed the $L1_2$ structure of γ' precipitates.

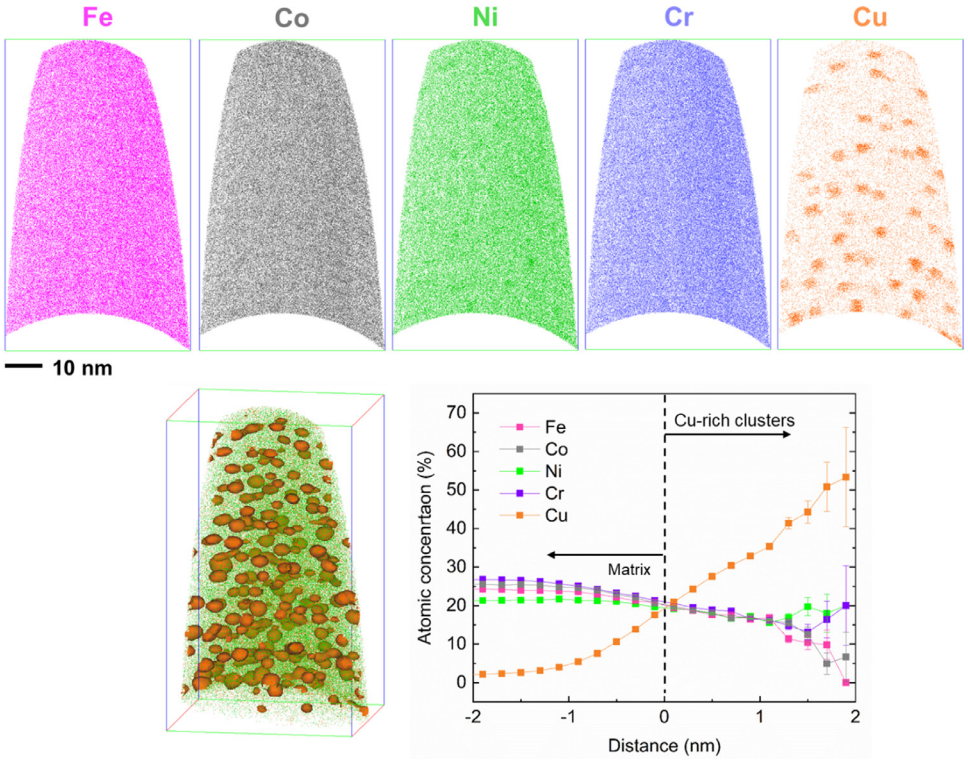

Fig. 3. APT analysis for the Cu-addition HEA irradiated at 973 K. The upper images (from left to right) displayed the 5 nm-thick sliced atom maps for Fe, Co, Ni, Cr, Cu. The lower images showed the 3D atom map with 10 at% Cu iso-concentration surface highlighted by green, and the average 1D composition proxigrams for the Cu-rich nanoclusters. (For interpretation of the references to color in this figure legend, the reader is referred to the web version of this article.)

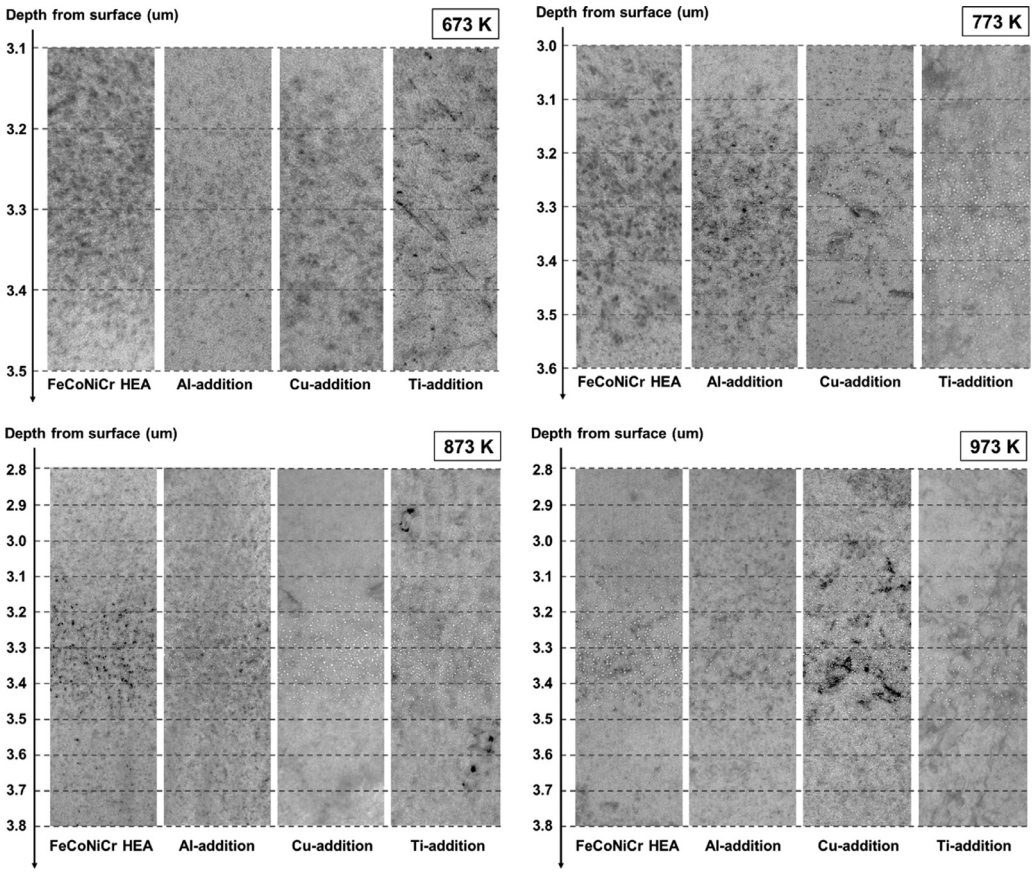

Fig. 4. A series of cross-sectional TEM images displaying He bubble formation along depth direction in the FeCoNiCr-based HEAs irradiated at different temperatures.

He bubble formation

He bubble behaviors including the distribution range, size, and number density were investigated for the FeCoNiCr-based HEAs irradiated at different temperatures. In Fig. 4, the cropped TEM images displayed the formation of He bubbles along irradiation depth, as a unit of temperature for different specimens. It showed that most of the bubbles were distributed near the peak damage region. And the variation of bubble density along depth direction has an analogous Gauss distribution that were roughly centering at the depth of ~3.3 um [33]. With increasing temperature, the distribution ranges became broader. If we considered a limitation for bubble detection ($< 10^{20}/m^3$), the maximum distribution length is about ~400 nm at 673 K, ~600 nm at 773 K, ~800 nm at 873 K and ~1000 nm at 973 K, beyond this range few bubbles were observed. At a given temperature, the distribution situations were different for the four HEAs. Comparing to the parent alloy, the minor alloying relatively dispersed He bubble formation, that the distribution range was broader by the sequence of Ti-, Cu-, Al-addition and FeCoNiCr HEA. This trend was universal for the four temperatures and the discrepancy was enlarged at a higher temperature. The quantitative analysis on the distribution length of He bubbles was provided in Fig. 6(a), in which the error bar was set as 10% reflecting the confidence of bubble detection.

The size and number density were another two indicators for He bubble behavior. In Fig. 5, the TEM images with the same magnification comparatively showed He bubbles in the peak damage region (depth from 3.2 to 3.4 um). The visual sense from these images was that He bubbles have a random and uniform arrangement in samples. In Fig. 6c, an analysis on the size distribution was given for each sample and revealed a monomodal distribution for them.

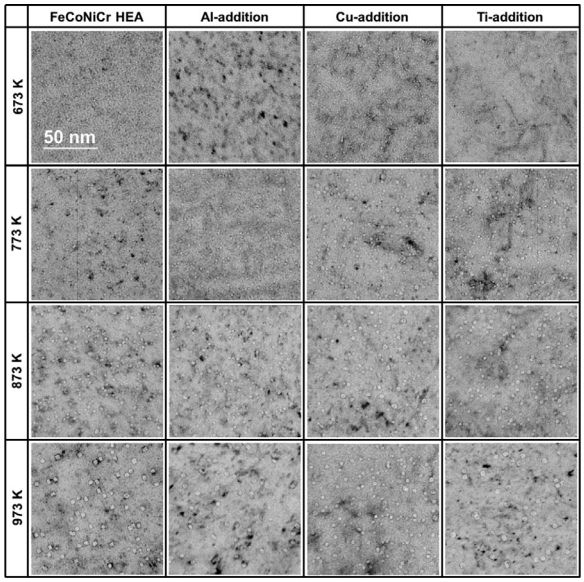

Fig. 5. Comparison for He bubbles formed in the peak damage region of FeCoNiCr-based HEAs irradiated at different temperatures. All the TEM images were taken at the same magnification and using the same defocus value.

The results implied that the bubble nucleation operated in a homogeneous way. The average bubble diameters and number density were summarized as a function of temperature, showing in Fig. 6b, d. It indicated a normal temperature-dependence for bubble evolution, that the size increased but density decreased with increasing temperature. At 673 K, the differences of bubble behavior were

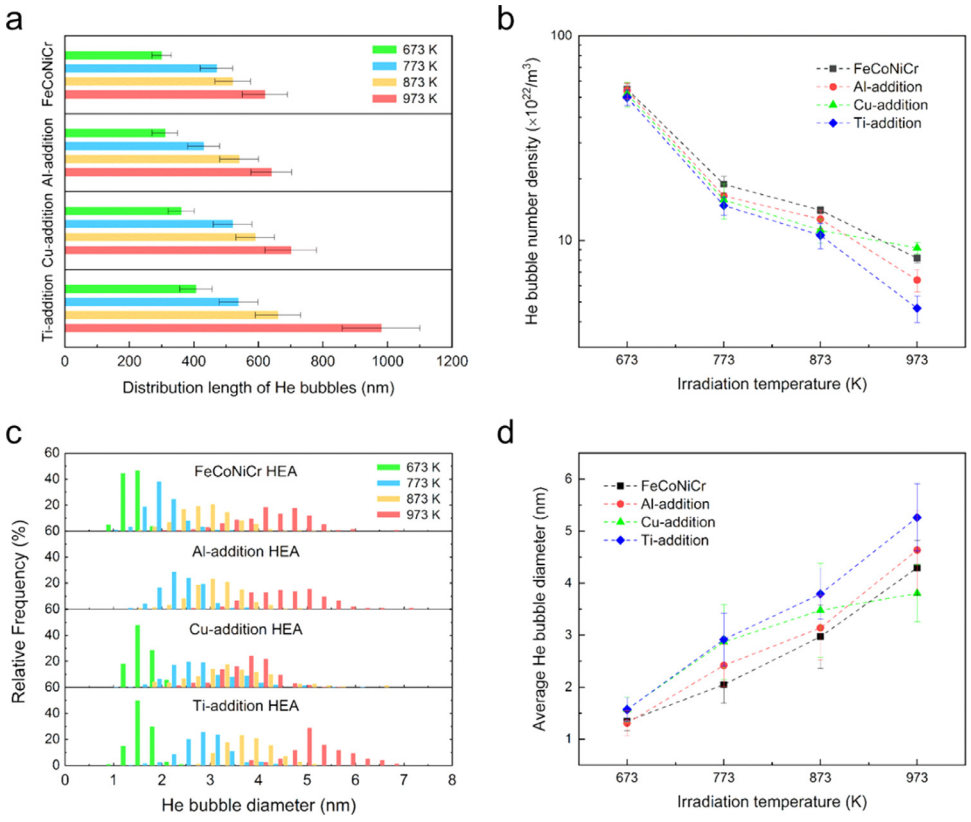

Fig. 6. Quantification for He bubbles in the FeCoNiCr-based HEAs irradiated at different temperatures. (a) for distribution length of He bubbles along depth direction; (b)–(d) for the number density, size distribution and average bubble diameter of He bubbles at the peak damage region, respectively.

Table 2
Volume swelling (%) induced by He bubbles in the FeCoNiCr-based HEAs irradiated by 2 MeV He ions at 673–973 K.

Irradiated materials	673 K	773 K	873 K	973 K
FeCoNiCr	0.070	0.085	0.193	0.314
$FeCoNiCrAl_{0.2}$	0.063	0.122	0.206	0.334
$FeCoNiCrCu_{0.2}$	0.088	0.165	0.247	0.265
$FeCoNiCrTi_{0.2}$	0.101	0.192	0.303	0.357

Table 3
Vacancy-dopant binding energies (eV) at 1NN position for different solute elements in Ni calculated by MD and DFT [57, 58].

	Fe	Cr	Al	Cu	Ti
Present MD	0.03	0.06	−0.19	−0.05	−0.09
DFT [57, 58]	0.02	0.06	0.00	−0.03	−0.06

quite small for the four HEAs. Their size was smaller than ~2 nm in diameter and the number density can reach ~5 × $10^{23}/m^3$. At 773 and 873 K, the influences of minor alloying began to be obvious, that bubbles had a larger size and lower density in the minor alloying HEAs comparing to that of the parent alloy. Such effects were more pronounced by the sequence of Ti, Cu, and Al-addition. When the irradiation temperature elevated to 973 K, He bubbles grew up to 4–6 nm in diameter and their density decreased to the magnitude of ~$10^{22}/m^3$. But the effect from Cu-addition was changed in which He bubbles had a smaller size and higher number density comparing to the parent alloy. The minor alloying influences of Ti and Al were similar with the low temperature situation, but the absolute difference of bubble size or density between the HEAs become larger. According to the mean bubble size and number density in the peak region, the volume swelling induced by He bubbles were further calculated in Table 2. The results showed that the minor alloying addition usually enhanced the bubble swelling except for the Cu-addition HEA irradiated at 973 K. It seems to be a bubble size dominated consequence.

Vacancy behaviors

With the referred potentials, the lattice constant of equiatomic FeCoNiCr alloy is determined as 3.56 Å, which is nearly same as the experimental value [56]. The elastic constants are calculated as C_{11}=167 GPa, C_{12}=134 GPa, and C_{44}=103 GPa, indicating the generated *fcc* supercell is elastically stable. To validate the potential in describing defect properties, we calculated the binding energies of a vacancy with a dopant in pure Ni at the first nearest-neighbor (NN) distance. The results are summarized in Table 3, together with the available results from density functional theory (DFT) calculations [57,58]. Unfortunately, there is no available data to compare for the considered quaternary system. It shows that the employed potential reproduces well the vacancy-dopant binding except for Al, where DFT predicts no interaction (0.00 eV) but the potential yields strong binding between them (0.19 eV). Therefore, in the following simulations we only presented the results for the systems of Cu, Ti-doped and pristine FeCoNiCr, which shall be reasonable to benchmark the energetics of vacancies in them.

To gain insight into the roles of minor alloying on vacancy behavior, we first analyzed the migration energies of vacancy before and after a doping element is added into the pristine FeCoNiCr. Vacancy diffusion was considered to proceed through jumps between two nearest neighboring (NN) lattice sites. In Fig. 7a and b, the energy barriers for each element migration are provided when a dopant (Cu or Ti) is located at the 1NN position from both vacancies. For reference, the migration energy of a single vacancy is 0.87 eV in pure Ni with this potential. The results show that

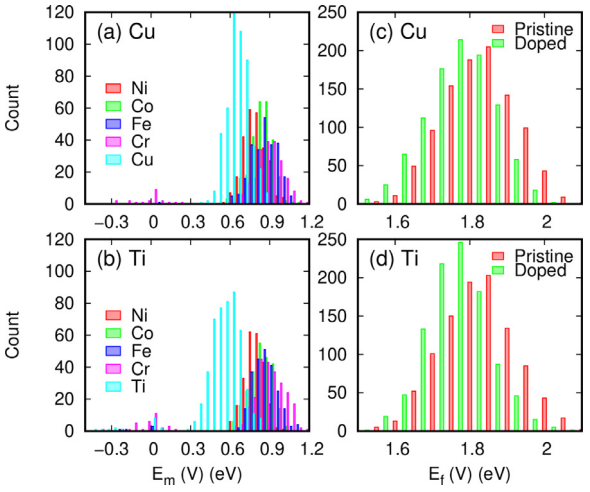

Fig. 7. Energetics of vacancies in the Cu (the first row) and Ti (the second row) doped FeCoNiCr systems. Left column (a, b): distribution of vacancy migration energies for each element in the doped systems. Right column (c, d): distribution of vacancy formation energies for the Cu, Ti-doped systems, in which black histogram indicates the values of pristine FeCoNiCr. One dopant was considered locating at the 1NN position from both vacancies.

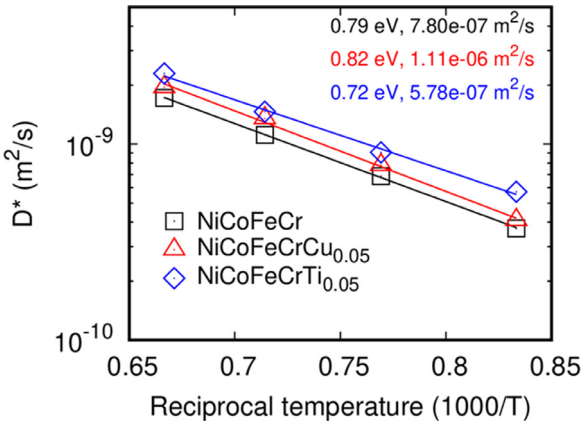

Fig. 8. Diffusion coefficient of a vacancy as a function of reciprocal temperature in pristine and doped-FeCoNiCr systems. The denoted activation energies and pre-factors were obtained from the Arrhenius fitting.

the migration barriers for 1NN jumps between vacancy-dopant are lower than that of vacancy-Ni jumps, vacancy-Co jumps, vacancy-Fe and vacancy-Cr jumps. Notably, jumps between vacancy-Ti exhibit the lowest barriers. It suggests that the energy barriers for vacancy diffusion could be reduced in the doped FeCoNiCr system. In addition, vacancy formation energy is an important quantity to measure the abundance of thermal vacancies during elevated-temperature irradiation. Fig. 7c and d shows the variation of vacancy formation energies after doping one Cu or Ti into the FeCoNiCr system. The dopant was considered locating at the similar 1NN situation and the values of pristine FeCoNiCr alloy were provided as black histogram. The results indicate that the doping Cu or Ti all tend to move the distributions of vacancy formation energies toward the low energy direction. It means that thermal vacancies are more readily activated in the doped systems. Such effect is also slightly pronounced by Ti-doping. Finally, Fig. 8 presented the diffusion coefficients of a vacancy in the considered alloys, which are fitted to the Arrhenius relation of $D = D_0 exp(-E_a/kT)$. The obtained activation energy of E_a and pre-factor D_0 were denoted in the plot. The results show that vacancy was more mobile in the minor alloying HEAs, while the minor alloying by Ti could more significantly facilitate vacancy diffusion in FeCoNiCr system.

Discussions

The experimental results indicated that the minor alloying addition in FeCoNiCr alloy could change He bubble behaviors, especially at a higher temperature irradiation. The atomistic simulation also revealed the different energy landscapes for vacancies after doping the Ti and Cu into the FeCoNiCr system. But how the featured vacancies influenced bubble evolution is still unclear. Here we would like to elucidate the effects of minor alloying on He bubble evolution, according to the theoretical framework proposed by Trinkaus [30,59].

He diffusion during irradiation

He diffusion is the basis of bubble formation. It is known that the mobility of He atoms under irradiation was controlled by the factors of temperature, the rate of He production and displacement damage [30]. The previous studies performed in the similar radiation damage suggested that He diffusion at the low temperature regime mainly operated by the replacement of self-interstitial atoms (SIAs) while the vacancy mechanism will dominate He migration at a high temperature [32,33]. The transition of two regimes usually occurred at the half-melting temperature of material [30]. Thus, in this study He diffusion at 673 and 773 K was expected through the replacement mechanism, in which He diffusivity can be taken as the value of vacancy:

$$D_{He} \cong D_V \text{ (Replacemnt mechanism)} \quad (1)$$

The simulation results indicated that the addition of Ti or Cu into FeCoNiCr system could enhance vacancy diffusion. Hence He atoms should share a higher diffusion rate in the minor alloying HEAs by the replacement mechanism. At the temperatures of 873 and 973 K, the vacancy concentration would be considerable so that He diffusion coefficient could be expressed as [60]:

$$D_{He} \cong C_V * D_V \text{(Vacancy mechanism)} \quad (2)$$

where C_V is the vacancy concentration and D_V is the vacancy diffusivity. During irradiation, the C_V was contributed by two sources of radiation induced vacancies and the thermal induced ones, but the weight of latter item will gradually be dominant with increasing temperature [61]. So the C_V at the high-temperature irradiation could be simply evaluated by the vacancy formation energy of E_V^F, which has been revealed in Fig. 7c and d. A lower E_V^F of minor alloying HEA means more abundant vacancies for He migration. By the vacancy mechanism, the different C_V would magnify the discrepancy of D_{He} between HEAs, which originally caused by the term of D_V at the low temperature situation. Therefore, the above analysis covering the two temperature regimes all suggested that the varied energetics of vacancy in the minor alloying HEAs can result in a higher He diffusivity comparing to their parent alloy.

The effect of minor alloying on the He diffusion could also get some clues from the TEM observations for He bubble distribution range. It is known that the implanted ions usually have a Gaussian distribution along the incident direction while the distribution will be broadened at the elevated temperatures due to the diffusion effect [62]. In this study, the temperature-dependent investigations verified this statement, showing that the He bubbles could form in a wider range at a higher temperature. Therefore, the comparison of bubble distribution range (Fig. 6a) at a given temperature should provide the information on He diffusion rate in the four HEAs. That is the Ti-addition could largely increase He mobility in the FeCoNiCr system while a weaker effect was given by the Cu and Al. Obviously, the experimental results have a good agreement with the suggestions drawn from simulation, that were previously restricted to the cases of Ti- and Cu-addition. Thus, the following

relation including the Al effect could be derived for our situation:

$$D_{\mathrm{He}}(\mathrm{Ti-addition}) > D_{\mathrm{He}}(\mathrm{Cu-addition}) > D_{\mathrm{He}}(\mathrm{Al-addition}) > D_{\mathrm{He}}(\mathrm{FeCoNiCr}) \quad (3)$$

Bubble nucleation and growth

He bubble formation is going on the two stages of nucleation and growth, such dynamic processes can be somewhat recorded by the observed bubble density and size. Based on the classical nucleation theory and the kinetic rate equations for the point defects, Trinkaus modeled the He bubble formation under an irradiation situation to probe the relationship between bubble characteristics and other factors [59,63]. In this framework, a di-atomic nucleation model was expected to govern the He bubble formation at the conditions of low temperature and/or high He production rate, in which He bubble number density (C_B) and bubble size (the average radius, $\overline{r_B}$) will comply the following relationships [59]:

$$C_B \propto \left[\left(D_{\mathrm{He}}^{eff}\right)^{-\beta} P_{He}^{2(\beta-\alpha)} t^{\beta-\alpha}\right]^{1/(3\beta-2\alpha)} \quad (4)$$

$$\overline{r_B} \propto \left(D_{\mathrm{He}}^{eff} P_{\mathrm{He}} t^2\right)^{1/(3\beta-2\alpha)} \quad (5)$$

where D_{He}^{eff} is the effective He diffusivity, P_{He} is the He production rate, t is the time for bubble evolution, and α, β are the constant depending on the bubble state. Since the simple He-vacancy complex was no longer thermally stable at the high temperature and/or low He production rate, a multi-atomic nucleation model was proposed to describe the He bubble evolution for this condition, as follows [59]:

$$C_B(t \to \infty) \sim 2C_B^* \propto \left(P_{\mathrm{He}}/t^{\gamma} c_{\mathrm{Hel}}^*\right)^{1/(\gamma+1)}/D_{\mathrm{Hel}} \quad (6)$$

$$\overline{r_B}(t \to \infty) \propto \left[D_{\mathrm{Hel}} {c_{\mathrm{Hel}}^*}^{1/(\gamma+1)} (P_{\mathrm{He}}/t^{\gamma})^{\gamma/(\gamma+1)} t^{\gamma+1}\right]^{1/\beta} \quad (7)$$

where c_{Hel}^* is the helium concentration in solution at nucleation peak, D_{Hel} is the He interstitial diffusion coefficient, and γ is the constant. The data reported in literatures [64–67] had demonstrated the availability of the two modes which successfully explained the He bubble behavior at different radiation scenarios over a wide temperature regime. In theory, the transition from the di-atomic nucleation to the multi-atomic nucleation occurred when the dissociation rate of a diatomic cluster being comparable to the rate of He absorption [66]. Our previous study proposed that He bubble formed in FeCoNiCr HEA should mainly operate by the di-atomic nucleation at 773–973 K, because of the high He production rate (~2 appm/s at the peak region). In this way, if we assigned the proper number for the constant and took the He production rate as the unit (due to the same irradiation time in this study) [59,67], a monotonic relationship between He diffusivity (D_{He}) and bubble behavior (C_B and $\overline{r_B}$) can be readily established. That is the $\overline{r_B}$ has a positive correlation to the D_{He} while it was negative for C_B. It signifies that when the minor alloying could enhance the He mobility in FeCoNiCr system, a lower nucleation number and larger growth were expected for He bubbles. The results fairly matched with our experimental observations except for the Cu-addition HEA irradiated at 973 K.

Effects of nanofeatures on He bubble evolution

It should be noted the above analysis were obtained based on the assumption that the bubble formation was given in a homogeneous system [30]. For the potential effects of nanofeatures in the matrix, some studies showed that He bubbles in the oxide dispersion strengthened (ODS) steels [68–70], usually have the high-density ultrafine structures. The interfaces between nanoclusters of Y-Ti-O and matrix were believed to be the effective trapping sites for mobile helium [71]. Similar trapping effect was also reported in the γ' strengthened Ni-based alloys [72–75]. However, more detailed investigations found that those ultrafine bubbles in ODS steels did not mostly attach to the nanoclusters [76,77], and they all have a uniform size either in matrix or on the surface of precipitates. It implied that the nanofeatures might affect the He bubble evolution through retarding He diffusion, rather than transform the bubble nucleation to a heterogenous way.

In our case, only the Ti-addition HEA possessed the nanofeatures of γ' precipitate before irradiation. But it failed to get a refining bubble structure comparing to other alloys, as indicated in Fig. 6d. The reasons might be twofold: the low-density precipitates (~10^{21}/m^3) did not provide enough sinks for He diffusion; and the strain fields surrounding coherent $L1_2$ phase are moderate for He trapping. This viewpoint was consist with the statement in [72]. Hence the Ti-enhanced He diffusion overwhelmed the effects of γ' precipitate. For the nanoclusters formed in the Cu-addition HEA irradiated at 973 K, although the lattice misfit between Cu-rich phase and matrix is also likely small, the extreme high-density of clusters could alternatively accommodate enough sink strength for He diffusion so that the trapping effects from nanofeatures surpassed the slightly enhanced He diffusion by Cu-addition. It might be the reason why bubble growth was relatively limited in this specimen (Fig. 6d), comparing to the FeCoNiCr parent alloy. Usually, the clustering rate of Cu-rich phase is mainly determined by the temperature. The limited coarsening of clusters at 973 K indicated that the kinetics of Cu-segregation should be slower at the other temperatures, in which the possible trapping effects from clusters were not prevailed during irradiation. Therefore, we believed that the nanofeatures would play an important role in the evolution of radiation defects when its density and/or lattice misfit were considerable.

Summary

In this study, the FeCoNiCr(Al/Cu/Ti)$_{0.2}$ HEAs and their parent FeCoNiCr alloy were irradiated by 2 MeV He$^+$ over a wide temperature regime from 673 to 973 K. After irradiation, their phase stability and He bubble behaviors were carefully examined by the conventional TEM method and APT. The energetics of vacancy and its diffusion coefficient in the considered systems were evaluated by MD simulation with proper potentials. Some findings can be summarized as follows:

a) The four HEAs could sustain their main phase structures at the given irradiation conditions (~0.3 dpa, 673–973 K). The ordering γ' precipitates in the Ti-addition HEA was more susceptible at a low temperature irradiation, while the nanosized Cu-rich clusters could densely form in the Cu-addition HEA at 973 K.
b) In general, He bubbles in the minor alloying HEAs had a wider distribution range, larger size and lower number density, comparing to that of parent alloy. Such effects were more significant at a higher irradiation temperature and more pronounced by the sequence of Ti-, Cu- and Al-addition.
c) The vacancy migration and formation energies of FeCoNiCr system could be reduced by doping Cu or Ti. At the doping-concentration of 5 at% nearly like our case, vacancy diffusion is more facilitated by Ti-doping.
d) In theory, more active vacancies could promote He diffusion by either the replacement or vacancy mechanism. So that a higher He diffusivity in the minor alloying HEAs was expected to enhance bubble growth and lower nucleation numbers during irradiation.
e) Except for the minor alloying effects on He diffusion, the nanofeatures of precipitate in matrix might greatly trap the mo-

bile He atoms when the nanofeatures' density and/or lattice misfit were considerable. It can account for the limited bubble growth in the Cu-addition HEA irradiated at 973 K.

Overall, this work not only provided a systematical investigation on He bubble formation in the FeCoNiCr-based HEAs, but also clearly figured out the factors controlling its evolution during irradiation. Even though the larger bubble size or lower number density is not always the desirable microstructure for nuclear structural materials, our study gains insights on tailoring radiation effects of multicomponent alloys through the minor alloying strategy.

Declaration of Competing Interest

The authors declare that they have no known competing financial interests or personal relationships that could have appeared to influence the work reported in this paper.

CRediT authorship contribution statement

Da Chen: Conceptualization, Investigation, Writing - original draft. **Shijun Zhao:** Methodology, Investigation, Writing - review & editing. **Jianrong Sun:** Methodology, Investigation, Writing - review & editing. **Pengfei Tai:** Resources. **Yanbin Sheng:** Resources. **Guma Yeli:** Methodology, Investigation. **Yilu Zhao:** Validation. **Shaofei Liu:** Validation. **Weitong Lin:** Validation. **Wu Kai:** Validation. **Ji-Jung Kai:** Supervision, Project administration, Funding acquisition.

Acknowledgment

This work was supported by Hong Kong Research Grant Council (RGC) [Grant No. CityU 11212915, CityU 11205018 and CityU 21200919], City University of Hong Kong 9610425 and National Natural Science Foundation of China (NSFC) [Grant Nos. 91426304, 11427904, 11275005 and 11975193]. Guangdong Basic and Applied Basic Research Foundation (No. 2019A1515011528), and Shenzhen Basic Research Program (No. JCYJ20190808181601662).

Data availability

The raw/processed data required to reproduce these findings cannot be shared at this time as the data also forms part of an ongoing study.

Supplementary materials

Supplementary material associated with this article can be found, in the online version, at doi:10.1016/j.jnucmat.2020.152458.

References

[1] S.J. Zinkle, G. Was, Materials challenges in nuclear energy, Acta Mater. 61 (3) (2013) 735–758.
[2] J.W. Yeh, S.K. Chen, S.J. Lin, J.Y. Gan, T.S. Chin, T.T. Shun, C.H. Tsau, S.Y. Chang, Nanostructured high-entropy alloys with multiple principal elements: novel alloy design concepts and outcomes, Adv. Eng. Mater. 6 (5) (2004) 299–303.
[3] M.-H. Tsai, J.-W. Yeh, High-entropy alloys: a critical review, Mater. Res. Lett. 2 (3) (2014) 107–123.
[4] Y. Zhang, G.M. Stocks, K. Jin, C. Lu, H. Bei, B.C. Sales, L. Wang, L.K. Béland, R.E. Stoller, G.D. Samolyuk, M. Caro, A. Caro, W.J. Weber, Influence of chemical disorder on energy dissipation and defect evolution in concentrated solid solution alloys, Nat. Commun. 6 (2015) 8736.
[5] K. Jin, C. Lu, L. Wang, J. Qu, W. Weber, Y. Zhang, H. Bei, Effects of compositional complexity on the ion-irradiation induced swelling and hardening in Ni-containing equiatomic alloys, Scr. Mater. 119 (2016) 65–70.
[6] C. Lu, L. Niu, N. Chen, K. Jin, T. Yang, P. Xiu, Y. Zhang, F. Gao, H. Bei, S. Shi, M.-R. He, I.M. Robertson, W.J. Weber, L. Wang, Enhancing radiation tolerance by controlling defect mobility and migration pathways in multicomponent single-phase alloys, Nat. Commun. 7 (2016) 13564.
[7] Y.F. Ye, Y.H. Zhang, Q.F. He, Y. Zhuang, S. Wang, S.Q. Shi, A. Hu, J. Fan, Y. Yang, Atomic-scale distorted lattice in chemically disordered equimolar complex alloys, Acta Mater. 150 (2018) 182–194.
[8] Y. Zhang, S. Zhao, W.J. Weber, K. Nordlund, F. Granberg, F. Djurabekova, Atomic-level heterogeneity and defect dynamics in concentrated solid-solution alloys, Curr. Opin. Solid State Mater. Sci. 21 (5) (2017) 221–237.
[9] S. Zhao, T. Egami, G.M. Stocks, Y. Zhang, Effect of d electrons on defect properties in equiatomic NiCoCr and NiCoFeCr concentrated solid solution alloys, Phys. Rev. Mater. 2 (1) (2018) 013602.
[10] S. Zhao, Fluctuations in stacking fault energies improve irradiation tolerance of concentrated solid-solution alloys, J. Nucl. Mater. 530 (2020) 151886, doi:10.1016/j.jnucmat.2019.151886.
[11] S. Zhao, Y. Osetsky, A.V. Barashev, Y. Zhang, Frenkel defect recombination in Ni and Ni–containing concentrated solid–solution alloys, Acta Mater. 173 (2019) 184–194.
[12] T. Kato, H. Takahashi, M. Izumiya, Effects of systematic modification with oversized elements on void formation in 316L austenitic stainless steel under electron irradiation, Mater. Trans. JIM 32 (10) (1991) 921–930.
[13] D.J. Mazey, W. Hanks, J.M. Titchmarsh, The influence of silicon and helium on the microstructural stability of ion-irradiated incoloy DS alloys, J. Nucl. Mater. 160 (2) (1988) 153–165.
[14] F. Garner, Irradiation performance of cladding and structural steels in liquid metal reactors, Mater. Sci. Technol. (1994).
[15] D. Mazey, W. Hanks, The effect of Si, Al and Ti additions on the void swelling response of ion-irradiated PE16-base alloy, Materials for Nuclear Reactor Core Applications, 2v, British Nuclear Energy Society, United Kingdom, 1987.
[16] R.M. Boothby, Radiation Effects in Nickel-Based Alloys, Compre. Nucl. Mater., Elesvier, 2012, pp. 123–150.
[17] D.B. Miracle, O.N. Senkov, A critical review of high entropy alloys and related concepts, Acta Mater. 122 (2017) 448–511.
[18] Y. Tong, D. Chen, B. Han, J. Wang, R. Feng, T. Yang, C. Zhao, Y.L. Zhao, W. Guo, Y. Shimizu, C.T. Liu, P.K. Liaw, K. Inoue, Y. Nagai, A. Hu, J.J. Kai, Outstanding tensile properties of a precipitation-strengthened FeCoNiCrTi0.2 high-entropy alloy at room and cryogenic temperatures, Acta Mater. 165 (2019) 228–240.
[19] Y.L. Zhao, T. Yang, Y.R. Li, L. Fan, B. Han, Z.B. Jiao, D. Chen, C.T. Liu, J.J. Kai, Superior high-temperature properties and deformation-induced planar faults in a novel L12-strengthened high-entropy alloy, Acta Mater. 188 (2020) 517–527.
[20] B. Cao, T. Yang, W.-h. Liu, C.T. Liu, Precipitation-hardened high-entropy alloys for high-temperature applications: a critical review, MRS Bull. 44 (11) (2019) 854–859.
[21] W. Kai, F.P. Cheng, C.Y. Liao, C.C. Li, R.T. Huang, J.J. Kai, The oxidation behavior of the quinary FeCoNiCrSix high-entropy alloys, Mater. Chem. Phys. 210 (2017) 362–369.
[22] W. Kai, F.P. Cheng, F.C. Chien, Y.R. Lin, D. Chen, J.J. Kai, C.T. Liu, C.J. Wang, The oxidation behavior of a Ni2FeCoCrAl0.5 high-entropy superalloy in O2-containing environments, Corros. Sci. 158 (2019) 108093.
[23] S. Xia, M.C. Gao, T. Yang, P.K. Liaw, Y. Zhang, Phase stability and microstructures of high entropy alloys ion irradiated to high doses, J. Nucl. Mater. 480 (2016) 100–108.
[24] C. Lu, T. Yang, K. Jin, N. Gao, P. Xiu, Y. Zhang, F. Gao, H. Bei, W.J. Weber, K. Sun, Y. Dong, L. Wang, Radiation-induced segregation on defect clusters in single-phase concentrated solid-solution alloys, Acta Mater. 127 (2017) 98–107.
[25] T.-n. Yang, C. Lu, K. Jin, M.L. Crespillo, Y. Zhang, H. Bei, L. Wang, The effect of injected interstitials on void formation in self-ion irradiated nickel containing concentrated solid solution alloys, J. Nucl. Mater. 488 (2017) 328–337.
[26] D. Chen, Y. Tong, J. Wang, B. Han, Y.L. Zhao, F. He, J.J. Kai, Microstructural response of He + irradiated FeCoNiCrTi 0.2 high-entropy alloy, J. Nucl. Mater. 510 (2018) 187–192.
[27] Y. Zhang, M.A. Tunes, M.L. Crespillo, F. Zhang, W.L. Boldman, P.D. Rack, L. Jiang, C. Xu, G. Greaves, S.E. Donnelly, L. Wang, W.J. Weber, Thermal stability and irradiation response of nanocrystalline CoCrCuFeNi high-entropy alloy, Nanotechnology 30 (29) (2019) 294004.
[28] T. Yang, W. Guo, J.D. Poplawsky, D. Li, L. Wang, Y. Li, W. Hu, M.L. Crespillo, Z. Yan, Y. Zhang, Y. Wang, S.J. Zinkle, Structural damage and phase stability of Al0.3CoCrFeNi high entropy alloy under high temperature ion irradiation, Acta Mater. 188 (2020) 1–15.
[29] E.E. Bloom, S.J. Zinkle, F.W. Wiffen, Materials to deliver the promise of fusion power – progress and challenges, J. Nucl. Mater. 329-333 (2004) 12–19.
[30] H. Trinkaus, B.N. Singh, Helium accumulation in metals during irradiation – where do we stand? J. Nucl. Mater. 323 (2-3) (2003) 229–242.
[31] Y. Dai, G.R. Odette, T. Yamamoto, The effects of helium in irradiated structural alloys, Compr. Nucl. Mater., Elesvier, 2012, pp. 141–193.
[32] D. Chen, Y. Tong, H. Li, J. Wang, Y.L. Zhao, A. Hu, J.J. Kai, Helium accumulation and bubble formation in FeCoNiCr alloy under high fluence He+ implantation, J. Nucl. Mater. 501 (2018) 208–216.
[33] D. Chen, S. Zhao, J. Sun, P. Tai, Y. Sheng, Y. Zhao, G. Yeli, W. Lin, S. Liu, W. Kai, J.-J. Kai, Diffusion controlled helium bubble formation resistance of FeCoNiCr high-entropy alloy in the half-melting temperature regime, J. Nucl. Mater. 526 (2019) 151747.
[34] S. Zhao, D. Chen, J.-J. Kai, First-principles study of He behavior in a NiCoFeCr concentrated solid–solution alloy, Mater. Res. Lett. 7 (5) (2019) 188–193.
[35] B. Gwalani, V. Soni, D. Choudhuri, M. Lee, J.Y. Hwang, S.J. Nam, H. Ryu, S.H. Hong, R. Banerjee, Stability of ordered L1 2 and B 2 precipitates in face centered cubic based high entropy alloys – Al 0.3 CoFeCrNi and Al 0.3 CuFeCrNi 2, Scr. Mater. 123 (2016) 130–134.

[36] C.-M. Lin, H.-L. Tsai, H.-Y. Bor, Effect of aging treatment on microstructure and properties of high-entropy Cu0.5CoCrFeNi alloy, Intermetallics 18 (6) (2010) 1244–1250.
[37] T.-T. Shun, C.-H. Hung, C.-F. Lee, Formation of ordered/disordered nanoparticles in FCC high entropy alloys, J. Alloys Compd. 493 (1-2) (2010) 105–109.
[38] J.F. Ziegler, M.D. Ziegler, J.P. Biersack, SRIM–the stopping and range of ions in matter (2010), Nucl. Instrum. Methods Phys. Res. Sect. B 268 (11) (2010) 1818–1823.
[39] R.E. Stoller, M.B. Toloczko, G.S. Was, A.G. Certain, S. Dwaraknath, F.A. Garner, On the use of SRIM for computing radiation damage exposure, Nucl. Instrum. Methods Phys. Res. Sect. B 310 (2013) 75–80.
[40] L.A. Giannuzzi, J.L. Drown, S.R. Brown, R.B. Irwin, F.A. Stevie, Applications of the FIB lift-out technique for TEM specimen preparation, Microsc. Res. Tech. 41 (4) (1998) 285–290.
[41] S.M. Allen, Foil thickness measurements from convergent-beam diffraction patterns, Philos. Mag. A 43 (2) (1981) 325–335.
[42] S. Plimpton, Fast parallel algorithms for short-range molecular dynamics, J. Comput. Phys. 117 (1) (1995) 1–19.
[43] X.W. Zhou, R.A. Johnson, H.N.G. Wadley, Misfit-energy-increasing dislocations in vapor-deposited CoFe/NiFe multilayers, Phys. Rev. B 69 (14) (2004) 144113.
[44] Z. Lin, R.A. Johnson, L.V. Zhigilei, Computational study of the generation of crystal defects in a bcc metal target irradiated by short laser pulses, Phys. Rev. B 77 (21) (2008) 214108.
[45] G. Anand, R. Goodall, C.L. Freeman, Role of configurational entropy in body–centred cubic or face-centred cubic phase formation in high entropy alloys, Scr. Mater. 124 (2016) 90–94.
[46] F. Granberg, K. Nordlund, M.W. Ullah, K. Jin, C. Lu, H. Bei, L.M. Wang, F. Djurabekova, W.J. Weber, Y. Zhang, Mechanism of radiation damage reduction in equiatomic multicomponent single phase alloys, Phys. Rev. Lett. 116 (13) (2016) 135504.
[47] E. Levo, F. Granberg, C. Fridlund, K. Nordlund, F. Djurabekova, Radiation damage buildup and dislocation evolution in Ni and equiatomic multicomponent Ni-based alloys, J. Nucl. Mater. 490 (2017) 323–332.
[48] S.I. Rao, C. Woodward, T.A. Parthasarathy, O. Senkov, Atomistic simulations of dislocation behavior in a model FCC multicomponent concentrated solid solution alloy, Acta Mater. 134 (2017) 188–194.
[49] S. Zhao, On the role of heterogeneity in concentrated solid-solution alloys in enhancing their irradiation resistance, J. Mater. Res. 35 (2020) 1103–1112.
[50] G. Henkelman, B.P. Uberuaga, H. Jónsson, A climbing image nudged elastic band method for finding saddle points and minimum energy paths, J. Chem. Phys. 113 (22) (2000) 9901–9904.
[51] K.C. Russell, Phase instability under cascade damage irradiation, J. Nucl. Mater. 206 (2) (1993) 129–138.
[52] B. Han, J. Wei, Y. Tong, D. Chen, Y. Zhao, J. Wang, F. He, T. Yang, C. Zhao, Y. Shimizu, K. Inoue, Y. Nagai, A. Hu, C.T. Liu, J.J. Kai, Composition evolution of gamma prime nanoparticles in the Ti-doped CoFeCrNi high entropy alloy, Scr. Mater. 148 (2018) 42–46.
[53] G. Yeli, D. Chen, K. Yabuuchi, A. Kimura, S. Liu, W. Lin, Y. Zhao, S. Zhao, J.-J. Kai, The stability of γ' precipitates in a multi-component FeCoNiCrTi0.2 alloy under elevated-temperature irradiation, J. Nucl. Mater. 540 (2020) 152364.
[54] F. He, Z. Wang, B. Han, Q. Wu, D. Chen, J. Li, J. Wang, C.T. Liu, J.J. Kai, Solid solubility, precipitates, and stacking fault energy of micro-alloyed CoCrFeNi high entropy alloys, J. Alloys Compd. 769 (2018) 490–502.
[55] Y.F. Ye, Q. Wang, Y.L. Zhao, Q.F. He, J. Lu, Y. Yang, Elemental segregation in solid-solution high-entropy alloys: Experiments and modeling, J. Alloys Compd. 681 (2016) 167–174.
[56] Y. Tong, K. Jin, H. Bei, J.Y.P. Ko, D.C. Pagan, Y. Zhang, F.X. Zhang, Local lattice distortion in NiCoCr, FeCoNiCr and FeCoNiCrMn concentrated alloys investigated by synchrotron X-ray diffraction, Mater. Des. 155 (2018) 1–7.
[57] J.D. Tucker, Solute-vacancy interactions in nickel, MRS Proc. 1645 (2014) mrsf13-1645-ee08-08.
[58] J.D. Tucker, R. Najafabadi, T.R. Allen, D. Morgan, Ab initio-based diffusion theory and tracer diffusion in Ni–Cr and Ni–Fe alloys, J. Nucl. Mater. 405 (3) (2010) 216–234.
[59] H. Trinkaus, Modeling of helium effects in metals: High temperature embrittlement, J. Nucl. Mater. 133 (1985) 105–112.
[60] G.S. Was, Fundamentals of Radiation Materials Science: Metals and Alloys, Springer, 2016.
[61] K.C. Russell, Phase stability under irradiation, Prog. Mater Sci. 28 (3) (1984) 229–434.
[62] H. Ryssel, I. Ruge, Ionenimplantation, Springer-Verlag, 2013.
[63] H. Trinkaus, Energetics and formation kinetics of helium bubbles in metals, Radiat. Eff. 78 (1-4) (2006) 189–211.
[64] C. Zhang, K. Chen, Y. Wang, J. Sun, D. Shen, Formation of bubbles in helium implanted 316L stainless steel at temperatures between 25 and 550°C, J. Nucl. Mater. 245 (2-3) (1997) 210–216.
[65] Y.S. Wang, K.Q. Chen, C.H. Zhang, J.M. Quan, J.G. Sun, Z.Y. Zhao, The study of bubble formation in 316L stainless steel irradiated with helium ions at 873 K, J. Nucl. Mater. 240 (1) (1996) 70–74.
[66] B. Singh, H. Trinkaus, An analysis of the bubble formation behaviour under different experimental conditions, J. Nucl. Mater. 186 (2) (1992) 153–165.
[67] V. Zell, H. Schroeder, H. Trinkaus, Helium bubble formation in nickel during hot implantation, J. Nucl. Mater. 212 (1994) 358–363.
[68] C.M. Parish, K.A. Unocic, L. Tan, S. Zinkle, S. Kondo, L.L. Snead, D.T. Hoelzer, Y. Katoh, Helium sequestration at nanoparticle-matrix interfaces in helium+ heavy ion irradiated nanostructured ferritic alloys, J. Nucl. Mater. 483 (2017) 21–34.
[69] C. Lu, Z. Lu, R. Xie, C. Liu, L. Wang, Microstructure of HIPed and SPSed 9Cr-ODS steel and its effect on helium bubble formation, J. Nucl. Mater. 474 (2016) 65–75.
[70] T. Yamamoto, Y. Wu, G. Robert Odette, K. Yabuuchi, S. Kondo, A. Kimura, A dual ion irradiation study of helium–dpa interactions on cavity evolution in tempered martensitic steels and nanostructured ferritic alloys, J. Nucl. Mater. 449 (1-3) (2014) 190–199.
[71] L. Yang, Y. Jiang, Y. Wu, G.R. Odette, Z. Zhou, Z. Lu, The ferrite/oxide interface and helium management in nano-structured ferritic alloys from the first principles, Acta Mater. 103 (2016) 474–482.
[72] A. Czyrska-Filemonowicz, W. Kesternich, Helium bubble formation in model nickel-base alloys, J. Nucl. Mater. 137 (1) (1985) 33–43.
[73] A. Czyrska-Filemonowicz, A.A. Gadalla, B. Weckermann, W. Kesternich, Microstructure of helium-implanted Nimonic PE16, J. Nucl. Mater. 150 (1) (1987) 24–30.
[74] H. Shiraishi, A. Hasegawa, Helium effects in iron- and nickel-base developmental alloys, J. Nucl. Mater. 155-157 (1988) 1049–1053.
[75] C.D. Judge, N. Gauquelin, L. Walters, M. Wright, J.I. Cole, J. Madden, G.A. Botton, M. Griffiths, Intergranular fracture in irradiated Inconel X-750 containing very high concentrations of helium and hydrogen, J. Nucl. Mater. 457 (2015) 165–172.
[76] Q. Li, C.M. Parish, K.A. Powers, M.K. Miller, Helium solubility and bubble formation in a nanostructured ferritic alloy, J. Nucl. Mater. 445 (1-3) (2014) 165–174.
[77] P.D. Edmondson, C.M. Parish, Y. Zhang, A. Hallén, M.K. Miller, Helium bubble distributions in a nanostructured ferritic alloy, J. Nucl. Mater. 434 (1-3) (2013) 210–216.